Applicability of Castration Model in Sex Difference Studies: Insights from Metabolome and Transcriptome Analyses

Jianjun Jiang[1,2]*, Na Ge[2], Yuzhi Wang[2], Juntao Qi[3], Guibiao Wen[3], Xiufen Gu[2], Xuewen Yu[4], Muming Shao[4], Yueming Luo[4,5], Kangshuyun Gu[2], Feng Lin[3], Shudong Yang[2]*, and Wei Wei [1]*

[1] Institute for Systems Biology, Seattle, USA;
[2] Department of Nephrology, [3] Department of Urology, [4] Department of Pathology, [5]Department of Geriatrics, Shenzhen Traditional Chinese Medicine Hospital, The Fourth Clinical Medical College of Guangzhou University of Chinese Medicine, Shenzhen, China;

*Corresponding authors:
Jianjun Jiang, Ph.D., E-mail: jjiang@systemsbiology.org
Shudong Yang: ysd0870@gzucm.edu.cn
Wei Wei, Ph.D., E-mail: wwei@systemsbiology.org;

ABSTRACT

Background

Sex, as a critical biological variable, has historically been underappreciated, despite the pervasive influence of sexual dimorphism across physiological and pathological processes. A significant obstacle to advancing sex-biased biological research is the absence of an effective animal model. In recent years, castration has emerged as a potential model for elucidating sex-based differences in the context of healthy aging, where it has been shown to equalize lifespan and growth trajectories in genetically diverse mice. However, the molecular shifts induced by castration in common laboratory models, such as C57BL/6 mice, and the broader applicability of this model to other sex-related biological contexts remain largely unexplored.

Methods

We employed multi-omics and observational analyses to investigate the molecular changes associated with sex and sex hormones following castration. We analyzed serum, kidney, and liver samples from 12-week-old and 18-month-old castrated male C57BL/6 mice, alongside intact male and female counterparts. The castration model was further applied to assess differences in cisplatin-induced toxicity and age-related cognitive decline in comparison to unaltered controls.

Results

LC-MS/MS metabolomics revealed that castrated males exhibited substantial alterations in steroid hormone levels and increased concentrations of antioxidant compounds, such as taurine, despite identical diets. Integrated metabolome-transcriptome analysis confirmed distinct patterns of lipid peroxidation and oxidative stress across sham-operated female, male, and castrated male mice. Histopathological evaluations following cisplatin treatment and aging-related behavioral tests demonstrated the model's utility in investigating sex-dependent drug toxicity and cognitive decline. These findings underscored the critical role of sex hormones in modulating both toxicity defense mechanisms and cognitive performance.

Conclusion

This study provides a systematic multi-omics spectrum on the castration model and demonstrates its capacity to feminize metabolic and transcriptomic profiles, establishing it as a valuable tool for exploring sex hormone-driven biological differences. Our findings lay the groundwork for further mechanistic studies and broaden the potential applications of the castration model in diverse biomedical

research domains.

INTRODUCTION

Sex is an fundamental variable that shapes physical, psychological, cognitive, and behavioral traits[1]. It exerts a significant influence on development, reproduction, and pathogenesis[2]. For instance, the incidence and survival rates of various cancers, along with their clinical phenotypes and treatment responses, exhibit marked sex-related differences[3, 4]. Physiological and immunological disparities between males and females further affect drug metabolism and toxicity during cancer therapies[5]. In aging studies, it has been well-established that women generally live longer than men, with consistent lower biological ages assessed by molecular biomarkers. However, there is a paradox that women experience a higher incidence of chronic, age-related degenerative diseases compared to men, despite their longer lifespan[6, 7]. Although awareness of sex-related differences in health and disease is rising, the molecular underpinnings of these differences remain underexplored.

A major challenge in studying sex differences lies in the lack of reliable animal models that can disentangle the complex effects of both genetic variability (such as the influence of X and Y chromosomes) and the actions of sex hormones[8]. Traditional approaches to compare males and females often fail to isolate these variables, leaving key mechanisms obscured. In recent years, castration has emerged as a potent model for elucidating the sex-based differences, particularly in healthy aging. Accumulating evidence suggests that castration can extend the lifespan across multiple mammal species. Notably, historical records indicate that Korean eunuchs had a lifespan extension of 14.4–19.1 years compared to their non-castrated counterparts of similar socio-economic status[9]. Similarly, in veterinary and livestock practices, spaying and castration are recommended for disease prevention and lifespan extension[10]. Despite the widespread applications of castration in these fields, comprehensive studies linking castration to broader biological and molecular sex differences remain sparse.

Recent studies have begun to shed light on the biological impact of castration. In 2021, Sugrue et al. provided the first evidence that castration slows the intrinsic aging process in sheep, as evidenced by a slower DNA methylation clock[11]. More recently, Jiang et al. demonstrated that prepubertal castration abolished the differences in lifespan and growth trajectories between male and female UM-HET3 mice, a genetically diverse strain[12]. While these findings offer valuable insights into the role

of castration in aging, the full extent of castration's role in other sex-relevant differences are largely unknown.

In this study, we present the first integrated multi-omics and behavioral analyses of castrated mice and their non-altered counterparts. Given that genome sequences retain the same pre- and post-castration, we hypothesize that the alterations in hormone spectrum and subsequent changes in the metabolome, transcriptome, and epigenome induced by castration could be pivotal in regulating sex dimorphism. To this end, we employed mass spectrometry-based metabolomics and deep RNA sequencing (RNA-seq) to extensively investigate the multifaceted aspects of sex-related differences associated with castration. Our results reveal several mechanistic insights, laying the groundwork for further detailed investigations and highlighting the potential of castration models as a robust tool for studying sex differences across diverse biological contexts.

RESULTS

Castration slowed body weight acquisition and affected the secretion of steroid hormone spectrum

To elucidate the molecular changes caused by castration, we employed multi-omics approaches to resolve the potential roles at both molecular and phenotypic levels (**Figure 1A)**. Young adult C57BL/6 mice were castrated at 8 weeks old (casM) and exhibited slower gaining of body weight post-castration, but attained similar body weights as the sham males (shamM) by 60 weeks (**Figure 1B)**. This pattern align with findings in prepubertal castration models using UM-HET3 mice (**Figure 1B)**. At 27-30 weeks of age, we assessed the food intake among the three groups of mice. The casM group exhibited reduced food consumption compared to both shamM and sham female mice (shamF) (**Figure 1C)**. This spontaneous reduction in food intake in casM may contribute to the slower body weight acquisition post-castration, and is particularly intriguing given the well-established benefits of dietary restriction for promoting healthy aging and longevity. Considering the potential impact of testosterone deprivation due to castration on the development of young adult mice, we measured their body length and found no significant difference between casM and sham (**Figure 1D**). Similarly, rectal temperature measurements revealed no significant differences among the three groups (**Figure 1E**). Notably, hair graying, a common aging marker in both mice and humans[13], was significantly delayed in casM compared to shamM at 13 months, indicating a more youthful phenotype in the castrated group (**Supplementary Figure 1A**).

Hormones, serving as vital chemical messengers, travel through from bloodstream to tissues for coordinating a range of biological functions, with their dysregulation impacting development[14], aging[15] and disease progression[16]. The effect of surgical castration, specifically the removal of the testes, leads to a marked reduction in testosterone (TS) levels. However, the broader hormone changes resulting from castration remain underexplored. Here, we employed ultra-high-performance liquid chromatography coupled with multiple reaction monitoring tandem mass spectrometry (UHPLC-MRM-MS/MS) to analyze 17 targeted steroid hormones (SHs) in the serum of casM, shamM and shamF mice, at four weeks post-operation.

Given the limited volume of mouse serum available for SH measurement, we could

133 only detect and compare 10 SH types across three groups. Notably, castration
134 significantly altered SH secretion in casM (**Figure 1F**). As expected, testosterone and
135 its more potent form, dihydrotestosterone, were remarkably reduced in CasM, to the
136 point of being barely detectable (**Figure 1G**). Intriguingly, CasM mice exhibited a
137 significant higher level of 17α-Hydroxyprogesterone (17α-OHP) (**Figure 1G**) and
138 lower androstenedione (A4) compared to shamM ($p < 0.05$) (**Figure 1G**). These
139 hormones, precursors to TS, might be part of a compensatory mechanism in response
140 to TS deprivation [17]. In addition, we observed slight increases in aldosterone (ALD)
141 and corticosterone (CORT) in casM, with p-values of 0.11 and 0.083, respectively
142 (**Supplementary Figure 2**). ALD, a mineralocorticoid, and CORT, a glucocorticoid,
143 are primarily produced by the adrenal cortex. Their upregulation may suggest an
144 activated stress response and changes in mineral and glucose homeostasis consequent
145 to TS deprivation.

146 To elucidate metabolites associated with TS, we conducted an untargeted
147 metabolomics analysis by LC-MS/MS on serum samples from three groups of mice,
148 four weeks post-operation. A total of 1495 compounds with MS^2 scores ≥ 0.3 were
149 identified. Notably, coexpression analysis revealed that 17 of these compounds, which
150 include 11 bioactive lipids, showed a significant correlation with TS levels ($|r| \geq 0.8$, p
151 ≤ 0.001, **Figure 1H**), These 11 lipids encompass a range of molecules such as
152 prostaglandin B2 (PGD2), a specific phosphatidylcholine (PC) variant,
153 lysophosphatidylserine (LPS), lysophosphatidic acid (LPA), cyclic PA (CPA),
154 glucuronosyldiacylglycerol (GlcADG), sulfurHexosylceramide (SHexCer), and four
155 types of ceramide fatty acids (Cer) (**Supplementary Table 1**). While further
156 investigation is required to solidify these findings, our coexpression analysis suggests
157 that TS deprivation may significantly influence peripheral lipid metabolism,
158 particularly impacting ceramide and lysophosphatide pathways.

159 **Characterization of sex-related serum metabolomic features**

160 To assess the serum metabolomic profile differences among shamM, shamF, and CasM
161 mice at 12 weeks old (12w, 4 weeks post sham/castration procedures), principal
162 component analysis (PCA) was performed using data from 1495 compounds identified
163 by LC-MS/MS (**Figure 2A**). Lipid and lipid-like molecules constituted the largest
164 category (~33%) of these compounds (**Figure 2B**). A comparison of shamM and shamF
165 groups to explore sex-specific differences in serum metabolic activity revealed 255

166 significantly altered metabolites (SAMs) were identified (**Supplementary Table 2**),
167 with the top SAMs (ranked by fold changes) displayed in **Supplementary Figure 3A.**
168 Despite all mice receiving the same diet, we observed notably higher levels of
169 antioxidants and anti-inflammatory compounds in shamF compared to shamM. These
170 compounds, likely derive from food intake, included carnosic acid[18], arachidonic acid[19],
171 choline[20], nicotinamide[21], D-pantothenic acid[22], gamma-crocetin[23], ruscogenin[24], 4-
172 hydroxycinnamic acid[25], and oleamide[26, 27] (**Figure 2C).** Conversely, shamM mice
173 exhibited elevated levels of metabolites associated with resistance to high-fat diet-
174 related diseases, such as 5-HEPE[28] and 12-HEPE[29], and a higher level of protective L-
175 Anserine[30] than shamF (**Figure 2C**). Consistently, obesity-related compounds such as
176 LysoPE(0:0/20:3(11Z,14Z,17Z)/0:0) (LysoPE)[31] and 7−Ketocholesterol (7-KC)[32] were
177 found to be lower in male (**Figure 2C)**, offering insights into why obesity is more
178 prevalent in women than men[33].

179 Differential abundance (DS) score of the 255 SAMs was calculated to inform the
180 overall changes of each pathway (Figure 3D). These SAMs were found to be highly
181 enriched in lipid metabolism related pathways such as "sphingolipid signaling
182 pathway", "regulation of lipolysis in adipocytes" and "arachidonic acid metabolism",
183 suggesting a sex dimorphism in lipid metabolism. Additionally, a serum untargeted
184 metabolomic analysis in the same groups at 18 months old identified 868 compounds,
185 with "lipid and lipid-like molecules" again being the predominant category"
186 (**Supplementary Figure 3B**). PCA analysis suggested that the metabolic profile of 18-
187 month-old casM mice closely resembled that of shamF (**Supplementary Figure 3C**).
188 Similar to the younger mice, older shamF demonstrated higher levels of protective
189 compounds derived from the same diet compared to shamM **(Supplementary Figure**
190 **3D and Supplementary Table 3**), suggesting a potentially stronger ability in females
191 to generate healthy compounds from the same chow.

192 **Metabolomic feminization and taurine enrichment in castrated male mice**

193 In our analysis of 12-week-old mice serum, a comparative study between casM and
194 shamF mice identified 170 SAMs. In contrast, comparisons of "casM *vs* shamM" and
195 "shamF *vs* shamM" revealed 280 and 255 SAMs, respectively (**Figure 3A,**
196 **Supplementary Table 4**). Hierarchical Clustering of the 1495 identified compound
197 demonstrated a closer metabolic profile between casM and shamF than between casM
198 and shamM (**Figure 3B**). These findings, achieved without altering genetic background,

199 suggest that castration feminizes the metabolomic traits of male mice. When ranking
200 these SAMs by fold change (FC), notable differences were observed between shamM
201 and casM. The most significantly upregulated metabolite in casM was the unsaturated
202 fatty acid, PI (16:1/18:2), with log_2FC of 13.14, while the most downregulated was
203 guanosine, with a log_2FC of -6.79. CasM mice exhibited elevated levels of various
204 metabolites associated with healthy aging, anti-skin aging, and anti-inflammation, such
205 as ectoine[34], resolvin D2[35], oleamide[26, 27], taurine[36], taurocholic acid[37],
206 taurodeoxycholic acid[38], nicotinamide[39], ascorbic acid (vitamin C) [40], D-pantothenic
207 acid (vitamin B5)[41, 42] and choline[43] (**Figure 3C**). Similar to shamF, casM mice also
208 showed an enrichment of anti-oxidative metabolites likely derived from plant-based
209 foods, including ganoderenic acid C[44], oleuropeic acid[45], fasciculol C[46], graveoline[47]
210 (**Figure 3C**).

211 Enrichment analysis of the 280 SAMs from the "casM *vs* shamM" comparison
212 categorized them into pathways such as "bile secretion", "vitamin digestion and
213 absorption", "HIF-1 signaling pathway", "pyrimidine metabolism", various fatty acid
214 metabolism pathways including "arachidonic acid metabolism" and "regulation of
215 lipolysis in adipocytes" (**Figure 3D**). Interestingly, lipid metabolism-related pathways
216 were consistently enriched in both the "casM *vs* shamM" and "shamF *vs* shamM"
217 comparisons, indicating a potential sensitivity of lipid metabolism to the levels of SHs.

218 To investigate the metabolomic changes particularly derived from castration,
219 union SAMs among 12w-old casM, shamM and shamF groups were further classified
220 by c-means fuzzy clustering (**Figure 3E**, **Supplementary Table 5**). This analysis
221 revealed that cluster1 metabolites were notably elevated in casM compared to both
222 shamM and shamF. Topology-based pathway enrichment analysis indicated that
223 cluster1 metabolites were significantly ($p < 0.05$) enriched in pathways like "primary
224 bile acid biosynthesis", "D-glutamine and D-glutamate metabolism", "taurine and
225 hypotaurine metabolism" among others (**Figure 3F**). Notably, taurine levels were
226 higher in shamF than in shamM, and castration further augmented taurine levels along
227 with two key components of the taurine and hypotaurine metabolism pathway:
228 taurodeoxycholic acid (TDCA) and taurocholic acid (TCA) (**Figure 3G**). However, in
229 18m-old mice, a higher level of taurine with no significant changes of TDAC and TCA
230 were observed in shamM compared to shamF and casM, (**Figure 3H**), suggesting an
231 age-related sex dimorphism of taurine concentrations in mice serum. Bile acids (BA)

232 are crucial for maintaining lipid homeostasis and have been recognized as significant
233 signaling molecules during aging process[47]. Given that the SAMs from both "casM *vs*
234 shamM" and "shamF *vs* shamM" comparisons were significantly enriched in lipid-
235 related metabolic pathways, and the primary function of taurine is the conjugation of
236 cholesterol into bile acids[48], our findings suggest a potential link between taurine and
237 the sex and/or SH-related differences in lipid metabolism.

238 **Co-expression analysis across serum, livers and kidneys identifies potential**
239 **taurine-related regulators**

240 Kidney and liver are two major organs of organisms, the sex differences of renal and
241 hepatic function have been aware over years[49]. To elucidate the sex and age-related
242 regulatory networks in kidney and liver functions, we analyzed metabolome and
243 transcriptome of renal cortex and left liver lobe from three groups of mice at 12 week
244 (12w) and 18 months (18m) old. We detected an average of 899 compounds across both
245 tissues, with 121 compounds common among kidneys, livers and serum samples in both
246 age groups of sham, shamF, and casM mice (**Figure 4A** and **Supplementary Table 6**).
247 Coexpression analysis of these 121 commonly detected metabolites (CDMs) revealed
248 4 major clusters (**Figure 4B**). Metabolite Set Enrichment Analysis (MSEA) indicated
249 that Clusters 1, 2 and 3 are primarily involved in "Bile Acid Biosynthesis" and "Glycine
250 and Serine Metabolism" pathways (**Supplementary Figure 4A-C**). Notably, two
251 compounds known for their health-protective properties, taurine and alpha-linolenic
252 acid (ALA), were grouped in Cluster 4, suggesting a potential link between Cluster 4
253 compounds and healthy aging. Due to the limited range of lipids identifiable by KEGG
254 compounds database, Cluster 4 compounds were showing enrichment in a few terms
255 include "glyoxylate and dicarboxylate metabolism", "tyrosine metabolism" and others
256 (**Figure 4D**).

257 Considering the significance of taurine in aging and healthy aging, co-expression
258 analysis and c-means clustering were applied to identify genes that positively associated
259 with taurine. A total of 51 genes, whose expression levels showed similar dynamic trend
260 with taurine across casM, shamM and shamF mice in kidney and liver tissues at both
261 12w and 18m ages, were identified (**Figure 4E-G**). Among these, 15 genes exhibited a
262 generally decrease in expression in 18m tissues than 12w, such as *Hdac5, Preb, Plk2,*
263 *Atxn2* and *Trit* (**Figure 4E**). Two key lipid metabolism genes, *Srebf1* and *Ppard* were
264 among the 51 taurine-associated genes. *Srebf1* encodes sterol regulatory element-

binding protein 1 (SREBP1), a critical transcription factor regulating lipogenes involved in fatty acid and cholesterol biosynthesis[50]. *Ppard* encodes Peroxisome proliferator-activated receptor-delta (PPAR-δ), a member of the PPAR group in the nuclear receptor superfamily, known for its ligand-binding domains (LBD) that interacts with a broad range of lipid and lipid-like molecules[51]. This includes multiple types of polyunsaturated fatty acids, such as arachidonic and linoleic acid[51]. Both PPAR-δ and SREBP1 are also involved in retinoid X receptors/ Vitamin D Receptor (RXR/VDR) pathway (**Supplementary Table 7**). Given previous research showing that intestinal-specific deletion of VDR increased taurine levels[52], it is posited that taurine may also be associated with PPAR-δ and SREBP1 involved RXR/VDR pathway. Taken together, our results from both metabolomics and RNA-seq analysis strongly suggest that taurine is a key regulator in lipid peroxidation and metabolism, potentially playing a significant role in the process of healthy aging.

Joint metabolomic-transcriptomic analysis reveals a stronger capacity of defensing lipid peroxidation in female and castrated male

From deep RNA-seq analysis, we identified differentially expressed genes (DEGs) among casM, shamM and shamF groups in kidney and liver tissues (**Figure 5A-B, Supplementary Table 6**). In the kidneys of 12w old mice, over 4500 DEGs were noted in the comparisons of "shamF *vs* shamM" and "casM *vs* shamM," while only 987 genes showed differential expression between shamF and casM. Interestingly, livers seemed to be less affected by sex and/or the changes of SH levels than kidneys as only 2053 and 2533 DEGs were detected in “shamF *vs* shamM” and “casM *vs* shamM” comparisons, respectively, in 12w-old mice, and 546 DEGs between shamF and casM. Hierarchical clustering of RNA-seq data also revealed that the transcriptomic profiles of casM samples more closely resembled those of shamF than shamM samples, with the exception of 18m-old livers, suggesting a feminizing effect of castration that creates a crossover zone between male and female transcriptomic profiles in both kidney and liver (**Figure 5C**). However, the impact of sex and/or SH levels on transcriptomes, pronounced at 4 weeks post-castration, appeared to diminish in 18-month-old mice. In this older age group, the numbers of DEGs among the 3 groups were reduced, especially the comparisons of shamM with casM. In 18-month-old kidneys and livers of “casM *vs* shamM”, it showed only 435 and 353 DEGs, respectively.

Mapping the DEGs onto mouse chromosomes, we found that DEGs in "shamF *vs*

298 shamM" and "casM *vs* shamM" from both 12w and 18m-old liver tissues were
299 significantly clustered to chr4B3 (FDR < 0.05). Of the 145 annotated genes in chr4B3,
300 46 belong to the Major Urinary Proteins (*Mup*) family, with 25 being pseudogenes.
301 Except for *Mup4* and *Mup5*, which were barely detectable, the other *Mup* family genes
302 in chr4B3 were drastically reduced in casM and shamF livers, showing an average
303 log2FC = -5.57 (**Supplementary Figure 5A**). *Mup14*, *7*, *11*, and *1* were the top 4
304 differentially expressed *Mup* genes. It is known that *Mup* genes, predominantly
305 expressed in the liver, exhibit sexually dimorphic traits. Male mice typically excrete 2–
306 8 times more Mup protein in their urine compared to females [53]. Our results indicate
307 that the expression of *Mup* genes is influenced not only by sex genotypes but also by
308 testosterone levels.

309 To identify potential long-term salutary regulatory elements brought by sex and/or
310 castration at old age, we conducted a joint metabolomic-transcriptomic analysis. Here,
311 shamM mice, typically having a shorter liferspan, served as controls, while shamF and
312 casM mice, associated with healthier and longer lifespans, were the focus [54]. We utilized
313 the SAMs and DEGs from "shamF *vs* shamM" for the joint analysis to investigate
314 female-specific signatures; meanwhile, the joint metabolomic-transcriptomic analysis
315 was also performed using the SAMs and DEGs from "casM *vs* shamM" for interpreting
316 castration-specific features. In 18m-old kidneys, both shamF and casM groups showed
317 enrichment in KEGG programs related to "lysosome" and "cholesterol metabolism"
318 (**Supplementary Table 8-9**). In the liver of the same age group, the significantly
319 enriched KEGG pathways in the "casM *vs* shamM" comparison are illustrated in
320 **Figure 5D**. Notably, 20 terms, such as "linoleic acid metabolism", "arachidonic acid
321 metabolism", "retinol metabolism", "Jak-stat3 signaling" and "glutathione metabolism"
322 were consistent with those in the "shamF *vs* shamM" comparison (terms marked by
323 orange in **Figure 5D and 5E, Supplementary Table 10-11**). These KEGG terms are
324 known to play critical roles in lipid peroxidation.

325 To further validate these findings, we measured levels of malondialdehyde (MDA)
326 - a final product of polyunsaturated fatty acids peroxidation, in the three groups of mice.
327 Results indicated that shamF mice exhibited the lowest, while shamM mice had the
328 highest MDA levels in 18m-old livers, suggesting that females and castrated males
329 experience less lipid oxidation stress than their male counterparts (**Figure 5F**).
330 Additional oxidative stress markers, SOD1 and SOD2, were also tested and showed

similar trends to MDA among three groups (**Supplementary Figure 5B**). Taken together, our analysis suggests a close association between lipid metabolism and sex and SH levels. CasM and shamF mice are likely to absorb more health-beneficial compounds from their diet and experience reduced lipid peroxidative stress, potentially contributing to their longer lifespans.

Evaluating sex-dependent cisplatin toxicity through castration models

The clinical application of anti-tumor drugs, particularly Platinum-based drugs (PBDs) like cisplatin, which are used in nearly half of all chemotherapy treatments[55], is often hindered by drug-induced tissue toxicity. Notable adverse effects of these drugs include nephrotoxicity and hepatotoxicity, exhibiting differential impacts between male and female patients[56]. Such sex-dependent disparities in toxicity may be influenced by SHs, as suggested by the increased risk of nephrotoxicity observed in perimenopausal women undergoing cisplatin treatment[57]. Aging, a key factor influencing SH levels in both sexes, further complicates this relationship. To evaluate the utility of the castration model in studying the role of SHs in sex-dependent toxicity, we treated 12w-old mice (4 weeks post-castration/sham procedure) with a low dose of cisplatin twice, every 72 hours. Given that the kidney, and to a lesser extent the liver, are particularly vulnerable to cisplatin-induced damage, we conducted histological analyses on the renal cortex and left liver lobe tissues post-treatment.

Hematoxylin and eosin (H&E) staining of liver tissues showed the most severe liver injury in shamF mice, characterized by marked steatosis, sinusoidal congestion, and hemorrhage. In contrast, sham-operated male (shamM) and castrated male (casM) mice displayed comparatively less hepatic damage (**Figure 6A**). Conversely, Periodic Acid Schiff (PAS) staining of kidney tissues showed that casM mice had more severe kidney damages than both shamF and shamM, with a notable increase in acute renal tubule injury (**Figure 6B**). Previous studies on cisplatin-induced hepatotoxicity have yielded limited insights regarding sex differences. However, substantial evidence indicates that males are more susceptible to cisplatin-induced nephrotoxicity[56]. Studies administering cisplatin to rats at both 2 weeks (1 mg/kg/day) and a single dose (7.5 mg/kg) have shown that males experience more severe nephrotoxic effects than females[58]. Our pathological observations, combined with previous findings and the fact that castrated male (casM) mice have the lowest testosterone (TS) levels, suggest that intermediate TS levels, similar to those in shamF mice, may offer greater protection

364 against renal toxicity induced by cisplatin.

365 **Evaluating castration model in sex-dependent cognitive function**

366 Increasing evidence has revealed that cognitive function decline is sex-dependent, for
367 instance, a higher frequency of Alzheimer's diseases (AD) is reported for women than
368 men: nearly two-thirds of patients with AD are women[59]. However, the roles of SHs in
369 neurodegeneration process is rarely explored. Given the known correlation between
370 ages 10 – 14 months in mice and 38 – 47 years in humans, where senescence-related
371 changes become prominent[60], we conducted aging-related behavioral analyses among
372 the three groups of mice, to detect the potential roles of castration in cognitive function.
373 Barnes maze (BM), open field (OF) and novel object recognition (NOR) tasks were
374 tested to evaluate the spatial learning and memory, locomotor activity, and recognition
375 memory in 12 – 13 month-old casM, shamM and shamF mice (**Figure 7A**). Previous
376 studies have shown pronounced cognitive decline in middle-aged mice (8 – 12 months)
377 as assessed by the BM test[61]. However, our results showed that middle-aged casM
378 demonstrated superior performance, spending less time and making fewer errors with
379 less immobile time in locating the escape hole than shamM and/or shamF (**Figure 7B**).
380 Non-significant difference was found in OF and NOR tasks across the three groups
381 (**Supplementary Figure 6A-B**). Our results revealed that deprivation of TSs by
382 castration procedure can confer a protective effect against cognitive decline. This
383 selective enhancement in spatial learning and memory may reflect the differential
384 influence of castration on brain regions, particularly affecting areas like the
385 hippocampus that are crucial for navigation tasks, while exerting less impact on regions
386 involved in locomotor and recognition memory functions.

387

388 **DISCUSSION**

389 Recognizing and addressing sexual differences in both basic and clinical research is
390 critical, yet historically overlooked. On one hand, the bias toward using male subjects
391 in biomedical research has often been justified by the desire to minimize variability,
392 particularly traits influenced by the female estrous cycle[62]. This male-centric focus has
393 inadvertently limited our understanding of tissue function and disease mechanisms
394 from a sex-specific perspective, thereby highlighting the pressing need for more
395 inclusive animal models. On the other hand, straightforwardly comparing male with

396 female is generally applied in the increasingly emphatic but still limited sex-difference
397 studies, which made the leading mechanisms hard to recognize due to complicated
398 variables between male and female in both genetic and non-genetic aspects.

399 C57BL/6 mouse strain is one of the most widely used models in biomedical
400 research [63]. A systematic exploration of sex- and hormone-related molecular features
401 in this strain is crucial for advancing our understanding of sex-biased biological
402 processes. Moreover, it is critical to evaluate the utility of the castrated C57BL/6 model
403 in addressing sex-specific research questions.. In this study, we integrated observational
404 investigations, behavioral tests and multi-omics approaches to systematically
405 investigate the differences among shamM, casM and shamF C57BL/6 mice across
406 multiple tissues at different stages. We found that adult casM mice spontaneously
407 consumed less food than shamM, a behavior we believe to be the primary factor
408 contributing to their reduced rate of body weight gain. Considering the well-established
409 connection between dietary restriction, body weight, overall health, and longevity[64, 65],
410 it is plausible to suggest that this dietary pattern confers benefits for healthy aging in
411 casM mice. The underlying triggers prompting reduced food intake in casM mice merit
412 further investigation. Intriguingly, despite identical diet, shamF and casM mice
413 exhibited elevated levels of multiple food-derived health-promoting compounds
414 compared to shamM, including taurine, a compound that recently known for its aging-
415 slowing effects in various species[36]. These findings point to a potential influence of the
416 gut microbiome in modulating host metabolism and appetite regulation[66], which in turn
417 can affect eating behaviors and the bioavailability of beneficial compounds in food.
418 Given the dynamic interplay between the gut microbiome, aging, and its sex-dependent
419 modulation[67, 68], our results hint at the involvement of sex hormones in shaping the
420 microbial community. This, in turn, could influence dietary behaviors and the
421 assimilation of protective compounds from food. Future research delving into the
422 microbiota-gut-brain axis and its relationship with sex difference and healthy aging in
423 this castration model is warranted.

424 To broaden the feasibility and practicability of applying the castration model in
425 elucidating the molecular mechanisms of sex differences, we investigated the
426 differences in tissue injuries induced by tumor drugs and the cognitive differences
427 among three groups of mice. While more severe renal damages have previously been
428 observed in males compared to females following cisplatin treatment at both young and

429 old ages[69], the specific roles of genetic and non-genetic co-determinants in this disparity
430 are still elusive. Rostami et al. reported that rats, 1 week post-castration and treated with
431 a low dosage of TS rather than high dosage, exhibited increased tolerance to cisplatin
432 nephrotoxicity[70]. Complementing this, our pathological assays showed that castration
433 alone, without TS treatment, exacerbated renal toxicity. These findings collectively
434 suggest that balanced levels of TS are essential in defending against such toxicity. Given
435 that aging is a major contributor to changes in SH levels in both sexes[71, 72], and
436 considering the significant impact of these changes on chemotherapy-induced toxicities,
437 there is an imperative need for more comprehensive research to integrate these
438 hormonal alterations with chemotherapy toxicity across various age groups, thereby
439 enhancing the understanding and management of chemotherapy side effects in the aging
440 population.

441 Previous research has offered mixed insights into the impact of castration on
442 cognitive function. One such study employed a dual-task approach – utilizing an 8-arm
443 radial maze and a step-down avoidance task – to assess spatial and short-term memory
444 in rats. Conducted approximate 82 days post-surgical and chemical castration, the study
445 concluded that castration deteriorates memory function[73]. In contrast, our findings,
446 based on BM test in castrated mice, suggest an enhancement in cognitive performance.
447 Several factors could account for these divergent outcomes. First, the timing of
448 cognitive assessments post-castration differed between the studies. Our behavioral tests
449 were performed on 12-13month old mice, nearly 10-11 months after castration or sham
450 operations. It is plausible that the benefits of castration on spatial memory may not be
451 readily apparent in younger rodents but become more pronounced with age. Second,
452 the choice of behavioral tasks could also contribute to the observed discrepancies. The
453 step-down inhibitory avoidance task, employed in the previous study, uses immediate
454 electric shocks as stimuli to evaluate aversive memory, while the 8-arm radial maze
455 task requires deprivation of food and/or water for animals. Electric shock is a type of
456 psychological stress for rodents[74]. Mounting evidence suggests that testosterone
457 significantly modulates physiological responses to stressors[75]; thus, the markedly
458 reduced testosterone levels in castrated mice could potentially confound the evaluation
459 of cognitive performance. To mitigate potential confounders, we opted for less stressful
460 tasks – namely BM, OF and NOR tests. Our results from the BM test indicate that
461 castration may serve as a good model to study the roles of sex hormones in the sex

difference of cognitive function.

In summary, our study underscore the versatility of castration mouse model in sex-dependent biological queries. The model effectively "feminizes" males at multiple molecular levels through alterations in SHs, while preserving the somatic male genotype. This unique duality positions the castration model as a useful tool for distinguishing between hormone-induced sex differences and genotypic sex, broadening its utility beyond the scope of sex-biased research.

470 **METHODS**

471 **Animals, surgical castration procedures, and sample collections**

472 C57BL/6 mice were purchased from Zhuhai BesTest Bio-Tech Co,.Ltd. and housed in
473 the animal facility of Shenzhen TopBiotech Co., Ltd (Shenzhen, China) under
474 pathogen-free condition with free access to chow and water. Male and female mice at
475 8 weeks old were anesthetized by isoflurane for castration (testicles removed) or sham
476 procedures. Mice were placed on a warm pad after suture, then transferred to cages
477 while awake. 4-weeks post-castration/sham operations, serum was collected for steroid
478 hormone detection and untargeted metabolites analysis while liver and kidney were
479 dissected for untargeted metabolites analysis and RNA-seq (n=3-6/group).
480 Castrated/sham mice at 12-13m old were subjected to behavioral tests and were
481 sacrificed for sample collection at 18m. At 18m, serum was used for untargeted
482 metabolomics while liver and kidneys were dissected for both untargeted metabolomics
483 and RNA-seq (n=3-6/group). The animal study protocol was approved by the Animal
484 Ethics Review Board of Shenzhen TopBiotech Animal Facilities (No. TOP-IACUC-
485 2021-0100).

486 **Food intake, body length and rectal temperature measurement**

487 To investigate the potential link between reduced food intake and slower body weight
488 gain in castrated male mice (casM), we monitored the weekly changes in chow weight
489 over a 4-week period in 3 cages per group, each housing 3-5 mice aged 27 weeks. The
490 average food intake per mouse was calculated on a weekly basis. In assessing the impact
491 of castration on growth, we measured the body lengths of 29-week-old casM (n = 13),
492 shamM (n = 12), and shamF (n = 13) mice. Mice were gently extended to full length,
493 and measurements were taken from apex nasi to the base of the tail (tail not included).
494 Additionally, rectal temperature was measured on 30 weeks and 32 weeks old casM (n
495 = 13), shamM (n =12) and shamF (n = 13) mice, with the data combined for subsequent
496 analysis. Statistical differences in food intake, body length, and rectal temperature
497 across the three groups were evaluated using one-way ANOVA, multiple comparisons
498 with Tukey correction.

499 **Sample treatment for targeted steroid hormone spectrum detection**

500 50 μL serum was thawed and vortexed for 30s following by mixture with purified H_2O,
501 internal standard working solution and methanol. The well mixed samples were then

502 subjected to repeated 13000 rpm centrifuge for 10 minutes (mins) under 4°C. The
503 supernatant was retained further purified with OASIS PRiME HLB uElution (SPE).
504 200 μL methanol and 200 μL H_2O were separately used to wash and equilibrate the SPE
505 cartridges. The supernatant was loaded to the equilibrated cartridges and then washed
506 by 200 μL 10% ACN/H_2O (v/v) and 200 μL Hexane. The flow-through fraction was
507 discarded. Rinse the cartridge was with 40 μL 90% ACN/H_2O (v/v) and collect the
508 cluent. Add 60 μL H_2O to the cluent and shake the mixture for 3 mins. The final mixture
509 and the same volume of isotopically-labelled internal standards were subjected to
510 UHPLC-MS/MS analysis.

511 **Serum sample preparation for untargeted MS analysis**

512 150 μL methanol which was premixed with isotopically-labelled internal standard
513 compounds was added to 50 μL mouse serum and vortexed for 30 seconds to mix well.
514 The mixture was then sonicated for 10 mins in ice water bath and incubated for 1 h at -
515 40 °C to precipitate proteins. After 15-min high-speed centrifugation, the supernatant
516 was used for MS analysis. An equal aliquot of the supernatants obtained from each
517 serum sample was mixed as the quality control (QC).

518 **Kidney/liver sample preparation for untargeted MS analysis**

519 10-25 mg tissues were submerged with extraction solution (methanol:water = 3: 1, with
520 isotopically-labelled internal standard mixture) and homogenized in ice-water bath.
521 Incubate homogenized samples for 1 h at -40°C and centrifuge at 12000 rpm for 15 min
522 at 4°C. The supernatant was retained for MS analysis. A volume matched quality control
523 (QC) sample was prepared for MS.

524 **UHPLC-MS/MS analysis for targeted steroid hormone spectrum**

525 EXIONLC System (Sciex) equipped with a Waters Acquity Uplc Bch C8 column was
526 utilized for UHPLC analysis at Biotree Technology Co., Ltd, Shanghai, China. Assay
527 development was applied by SCIEX 6500+ triple quadrupole mass spectrometer (Sciex)
528 with an IonDrive Turbo V electrospray ionization (ESI) interface, under multiple
529 reaction monitoring (MRM) module. MassLynx Work Station Software (Version 4.1)
530 was employed for MRM data acquisition and preprocessing.

531 **UHPLC-MS/MS untargeted metabolomics analysis**

532 T3 chromatographic column with affinities to both lipid and hydrophile at Biotree

533 Technology Co., Ltd (Shanghai, China) was used to acquire the metabolome of
534 castrated male (casM), sham male (shamM) and sham female (shamF) mice by Orbitrap
535 mass spectrometer. Joint negative (NEG) and positive (POS) ionization modes were
536 employed for detecting metabolites based on their mass to charge ratios. Raw data was
537 converted to the mzXML format using ProteoWizard platform
538 (https://proteowizard.sourceforge.io/) and processed with an in-house R script and
539 XCMS tool[76] for peak detection, extraction, alignment, and integration. Data was
540 subjected to fragment extracted ion chromatogram (MS^2) annotations as previously
541 described[77], MS^2 metabolites with scores > 0.3 were retained for next-step analysis.
542 These compounds were mapped to Human Metabolome Database (HMDB) and
543 classified into multiple categories. The biggest category under both NEG and POS
544 modes is lipid and lipid-like molecules, which counts for ≥ 30% identified metabolites
545 (**Figure 2A-B, Supplementary Table 2-3**). Compounds from NEG and POS modes
546 were merged for down-stream analysis.

547 **RNA extraction for RNA-seq analysis**

548 Total RNA was extracted using Trizol reagents (Invitrogen Cat#15596026) as we have
549 described before[78]. PolyA-tailed RNA was enriched for constructing 150bp pair-end
550 RNA-sequencing libraries using MGISEQ-2000RS kit (MGI Cat#1000012555), and
551 sequenced by DNBseq MGI2000 platform at BGI genomics Co., Ltd, Shenzhen, China.

552 **Cisplatin administration**

553 Mice were administrated for intraperitoneal injection of cisplatin (Cat# 232120, sigma)
554 at 4 weeks post-castration/sham operations, with a dosage of 5 mg/kg every 72 hours
555 for 2 times. Mice were sacrificed 48 hours after cisplatin treatment for the collection of
556 liver and kidney tissues.

557 **Histopathological analysis**

558 For liver and kidney tissue examination, samples were first fixed in 10% formalin
559 solution for 48 hours, followed by paraffin embedding. Sections of 3 μm thickness were
560 then prepared for histological analysis. Hematoxylin and Eosin (H & E) and Periodic
561 Acid-Schiff (PAS) staining were performed according to established protocols. Liver
562 injury was evaluated by visually inspecting the patterns of steatosis, sinusoidal
563 congestion, and hemorrhage. Renal injury was quantitatively assessed using the scoring
564 criteria established in a previous study[79]. Statistical differences of renal injury scores

565 across the three groups were assessed one-way ANOVA (multiple comparisons with
566 Turkey correction).

567 **Western-blot**

568 Total protein was isolated on ice by cell & tissue lysis buffer (Cat#P0013, Beyontime,
569 China) and quantitated using BCA assay kit (Cat#P0012, Beyontime, China).
570 Approximate 15ug protein was used for western-blot assays following previous
571 protocols[80]. Antibodies for MDA, SOD1 and SOD2were purchased from abcam (Cat#
572 ab243066, ab13498 and ab13533), GAPDH was purchased from Beyontime (Cat#
573 AF0006).

574 **Behavioral tests**

575 Three groups of mice include casM, shamM and shamF at 12-13 months old (n= 6-13)
576 were subjected to BM, OF and NOR tasks. A 60 cm high, 120 cm-diameter and 60 mm
577 thick circular wheeled PVC slab with 25 cm-diameter holes was used for BM tests. A
578 modified protocol was employed following the standard methods in previous study[81].
579 Briefly, mice were firstly trained in continuous 7 days to find the escape hole within 4
580 mins; if failed, mice were finally guided to the target hole gently. Mice were subjected
581 to the probe trial on day 8. OF test was applied to test the exploratory behavior and
582 general activity of mice, mice were placed in an enclosure, rectangular tank with
583 surrounding walls for 5 mins, distance moved, time spent moving, rearing, and change
584 in activity over time for each mouse were recorded. NOR test was performed following
585 previous study[82]. Mice were placed in the empty tank for 10 mins on day1; day 2, two
586 objects were placed in the tank, and mice were allowed for 10 mins to explore; one of
587 the objects was replaced by a new one on day 3, and time spent for exploration (TE)
588 within 5 mins for each object was recorded. NOR index was calculated via this
589 formulation: NOR index = new object TE- old object TE/ Total TE. Mice behaviors
590 during these tests were recorded and analyzed by ANY-MAZE software
591 (https://www.any-maze.com/). Statistical differences in BM, OF and NOR tasks among
592 the three groups were analyzed via one-way ANOVA, multiple comparisons with
593 Turkey correction.

594 **Identification of significant altered metabolites (SAMs) and differentially**
595 **expressed genes (DEGs)**

596 A strict pipeline was applied to identify SAMs. Firstly, the normalized peak values of

597 metabolites were subjected to unsupervised principal component analysis (PCA) and
598 then administrated to supervised orthogonal projections to latent structures-
599 discriminate analysis (OPLS-DA) for data modeling by commercial SIMCA software
600 (V16.0.2). A 7-fold cross validation was employed for model selection. To evaluate the
601 predictive power and robustness of OPLS-DA model, a 200-times-permutations was
602 performed and the value of variable importance in the projection (VIP) of the first
603 principal component in OPLS-DA analysis was calculated which represents the
604 contribution of each variable to the model. Metabolites with VIP > 1 and students' t-
605 test *p*-value < 0.05 were recognized as SAMs. For DEG identification, quality control
606 was performed for raw RNA-seq reads by SolexaQA (-h 30, -l 30)[83]. Cleaned reads
607 were subjected to Hisat2[84] for mapping. Cufflinks package[85] was utilized to calculate
608 the Fragments Per Kilobase of transcript per Million mapped reads (FPKM) values and
609 to identify DEGs use FDR < 0.05 as the cutoff value.

610 **Expression trend clustering analysis**

611 To identify expression trend patterns of metabolites among the serum samples of 12w
612 casM, shamM and shamF, the union of SAMs across three pairwise comparisons in
613 **Figure 3E** were analyzed by Mfuzz package (c=9, m =1.25)[86]. To illustrate genes that
614 potentially related with taurine, the expression levels (FPKM values) of all the
615 annotated genes in kidneys and livers at 12w and 18m casM, shamM and shamF mice,
616 were also subjected to Mfuzz package[86] for clustering (c=9, m =1.25). The semi-
617 quantitative concentrations of taurine were plotted as stack lines. Genes that show
618 similar expression trend with taurine in all the tissues were retained (**Figure 4F-G**).

619 **Hierarchical clustering analysis**

620 Hierarchical clustering analysis for SH levels after castration/sham treatments (Figure
621 2A), the expression of 51 taurine related genes (**Figure 4E**), serum metabolomic
622 profiles among casM, shamM and shamF using (**Figure 3B**) and tissue RNA-seq gene
623 expression profiles (Figure 6C), were performed by Hclust function in R platform using
624 Euclidean distance metric and complete lineage. The z-score standardized SH levels
625 and expression levels of taurine related genes after clustering were visualized via
626 heatmap using pheatmap 1.0.12 package.

627 **Enrichment analysis of SAMs**

628 SAMs were subjected for topology-based KEGG pathway enrichment analysis using

MetaboAnalyst with default parameters[87]. Differential abundance (DA) scores[88] were calculated for the significant enrichment terms using this formula: DA scores = $\frac{\text{Up regulated metabolite No.in the pathway} - \text{Downregulated metabolite No. in the pathway}}{\text{Total metabolite No.of the pathway}}$

Joint metabolome & transcriptome analysis

To examine the interplay between metabolomics and other transcriptomics layers, SAMs and DEGs were used for joint metabolome & transcriptome enrichment analysis against KEGG pathways via MetaboAnalystR under joint-analysis module by hypergeometric test with default parameters. FDR < 0.05 was applied as the cut-off value.

REFERENCE

1. Ivan, S., Daniela, O. & Jaroslava, B.D. Sex differences matter: Males and females are equal but not the same. *Physiol Behav* **259**, 114038 (2023).
2. Waldhorn, I. et al. Modeling sex differences in humans using isogenic induced pluripotent stem cells. *Stem Cell Reports* **17**, 2732-2744 (2022).
3. Yang, M. et al. SexAnnoDB, a knowledgebase of sex-specific regulations from multi-omics data of human cancers. *Biol Sex Differ* **15**, 64 (2024).
4. Rubin, J.B. The spectrum of sex differences in cancer. *Trends Cancer* **8**, 303-315 (2022).
5. Kammula, A.V., Schäffer, A.A., Rajagopal, P.S., Kurzrock, R. & Ruppin, E. Outcome differences by sex in oncology clinical trials. *Nature Communications* **15**, 2608 (2024).
6. Hägg, S. & Jylhävä, J. Sex differences in biological aging with a focus on human studies. *eLife* **10**, e63425 (2021).
7. Fischer, K.E. & Riddle, N.C. Sex Differences in Aging: Genomic Instability. *The Journals of Gerontology: Series A* **73**, 166-174 (2018).
8. Ngun, T.C., Ghahramani, N., Sánchez, F.J., Bocklandt, S. & Vilain, E. The genetics of sex differences in brain and behavior. *Front Neuroendocrinol* **32**, 227-246 (2011).
9. Min, K.J., Lee, C.K. & Park, H.N. The lifespan of Korean eunuchs. *Curr Biol* **22**, R792-793 (2012).
10. Howe, L.M. Current perspectives on the optimal age to spay/castrate dogs and cats. *Vet Med (Auckl)* **6**, 171-180 (2015).
11. Sugrue, V.J. et al. Castration delays epigenetic aging and feminizes DNA methylation at androgen-regulated loci. *Elife* **10** (2021).
12. Jiang, N. et al. Prepubertal castration eliminates sex differences in lifespan and growth trajectories in genetically heterogeneous mice. *Aging Cell*, e13891 (2023).
13. Zhang, Z. et al. Wnt/β-catenin signaling promotes aging-associated hair graying in mice. *Oncotarget* **8**, 69316-69327 (2017).
14. Kraemer, W.J., Ratamess, N.A., Hymer, W.C., Nindl, B.C. & Fragala, M.S. Growth Hormone(s), Testosterone, Insulin-Like Growth Factors, and Cortisol: Roles and Integration for Cellular Development and Growth With Exercise. *Front Endocrinol (Lausanne)* **11**, 33 (2020).
15. van den Beld, A.W. et al. The physiology of endocrine systems with ageing. *Lancet Diabetes Endocrinol* **6**, 647-658 (2018).
16. Crafa, A. et al. The Burden of Hormonal Disorders: A Worldwide Overview With a Particular Look in Italy. *Front Endocrinol (Lausanne)* **12**, 694325 (2021).
17. Turcu, A., Smith, J.M., Auchus, R. & Rainey, W.E. Adrenal androgens and androgen precursors-definition, synthesis, regulation and physiologic actions. *Compr Physiol* **4**, 1369-1381 (2014).
18. Lin, C. et al. Effects on longevity extension and mechanism of action of carnosic acid in Caenorhabditis elegans. *Food Funct* **10**, 1398-1410 (2019).
19. Das, U.N. Ageing: Is there a role for arachidonic acid and other bioactive lipids? A review. *J Adv Res* **11**, 67-79 (2018).
20. Wortmann, S.B. & Mayr, J.A. Choline-related-inherited metabolic diseases-A mini review. *J Inherit Metab Dis* **42**, 237-242 (2019).
21. Igarashi, M. et al. Chronic nicotinamide mononucleotide supplementation elevates blood nicotinamide adenine dinucleotide levels and alters muscle function in healthy older men. *npj Aging* **8**, 5 (2022).

22. Hong, Y. et al. Association between plasma Vitamin B5 levels and all-cause mortality: A nested case-control study. *J Clin Hypertens (Greenwich)* **24**, 945-954 (2022).
23. Mohammadi, E., Mehri, S., Badie Bostan, H. & Hosseinzadeh, H. Protective effect of crocin against d-galactose-induced aging in mice. *Avicenna J Phytomed* **8**, 14-23 (2018).
24. Lu, H.J. et al. Ruscogenin ameliorates diabetic nephropathy by its anti-inflammatory and anti-fibrotic effects in streptozotocin-induced diabetic rat. *BMC Complement Altern Med* **14**, 110 (2014).
25. Sova, M. & Saso, L. Natural Sources, Pharmacokinetics, Biological Activities and Health Benefits of Hydroxycinnamic Acids and Their Metabolites. *Nutrients* **12** (2020).
26. Heo, H.J. et al. Effects of oleamide on choline acetyltransferase and cognitive activities. *Biosci Biotechnol Biochem* **67**, 1284-1291 (2003).
27. Ano, Y. et al. Preventive effects of a fermented dairy product against Alzheimer's disease and identification of a novel oleamide with enhanced microglial phagocytosis and anti-inflammatory activity. *PLoS One* **10**, e0118512 (2015).
28. Wang, C. et al. Hydroxyeicosapentaenoic acids and epoxyeicosatetraenoic acids attenuate early occurrence of nonalcoholic fatty liver disease. *Br J Pharmacol* **174**, 2358-2372 (2017).
29. Nagatake, T. et al. 12-Hydroxyeicosapentaenoic acid inhibits foam cell formation and ameliorates high-fat diet-induced pathology of atherosclerosis in mice. *Sci Rep* **11**, 10426 (2021).
30. Rokicki, J. et al. Daily Carnosine and Anserine Supplementation Alters Verbal Episodic Memory and Resting State Network Connectivity in Healthy Elderly Adults. *Front Aging Neurosci* **7**, 219 (2015).
31. Cai, H., Wen, Z., Meng, K. & Yang, P. Metabolomic signatures for liver tissue and cecum contents in high-fat diet-induced obese mice based on UHPLC-Q-TOF/MS. *Nutr Metab (Lond)* **18**, 69 (2021).
32. Anderson, A. et al. 7-Ketocholesterol in disease and aging. *Redox Biol* **29**, 101380 (2020).
33. Kanter, R. & Caballero, B. Global gender disparities in obesity: a review. *Advances in nutrition* **3**, 491-498 (2012).
34. Bilstein, A., Heinrich, A., Rybachuk, A. & Mösges, R. Ectoine in the Treatment of Irritations and Inflammations of the Eye Surface. *Biomed Res Int* **2021**, 8885032 (2021).
35. Zhao, M. et al. Resolvin D2 and its receptor GPR18 in cardiovascular and metabolic diseases: A promising biomarker and therapeutic target. *Pharmacol Res* **195**, 106832 (2023).
36. Singh, P. et al. Taurine deficiency as a driver of aging. *Science* **380**, eabn9257 (2023).
37. Warden, C., Barnett, J.M. & Brantley, M.A., Jr. Taurocholic acid inhibits features of age-related macular degeneration in vitro. *Exp Eye Res* **193**, 107974 (2020).
38. Wolf, P.G. et al. Effects of taurocholic acid metabolism by gut bacteria: A controlled feeding trial in adult African American subjects at elevated risk for colorectal cancer. *Contemp Clin Trials Commun* **19**, 100611 (2020).
39. Ur Rahman, S., Qadeer, A. & Wu, Z. Role and Potential Mechanisms of Nicotinamide Mononucleotide in Aging. *Aging Dis* (2023).

40. Harrison, F.E. A critical review of vitamin C for the prevention of age-related cognitive decline and Alzheimer's disease. *J Alzheimers Dis* **29**, 711-726 (2012).
41. Pelton, R.B. & Williams, R.J. Effect of pantothenic acid on the longevity of mice. *Proc Soc Exp Biol Med* **99**, 632-633 (1958).
42. Ishiguro, K. Aging effect of blood pantothenic acid content in female. *Tohoku J Exp Med* **107**, 367-372 (1972).
43. Dave, N. et al. Dietary choline intake is necessary to prevent systems-wide organ pathology and reduce Alzheimer's disease hallmarks. *Aging Cell* **22**, e13775 (2023).
44. Wang, J., Cao, B., Zhao, H. & Feng, J. Emerging Roles of Ganoderma Lucidum in Anti-Aging. *Aging Dis* **8**, 691-707 (2017).
45. Kim, Y.J. et al. Oleanolic Acid Protects the Skin from Particulate Matter-Induced Aging. *Biomol Ther (Seoul)* **29**, 220-226 (2021).
46. Ványolós, A. et al. Extracts and Steroids from the Edible Mushroom Hypholoma lateritium Exhibit Anti-Inflammatory Properties by Inhibition of COX-2 and Activation of Nrf2. *Chem Biodivers* **17**, e2000391 (2020).
47. Li, Z., Mu, C., Wang, B. & Jin, J. Graveoline Analogs Exhibiting Selective Acetylcholinesterase Inhibitory Activity as Potential Lead Compounds for the Treatment of Alzheimer's Disease. *Molecules* **21**, 132 (2016).
48. Murakami, S. et al. Taurine ameliorates cholesterol metabolism by stimulating bile acid production in high-cholesterol-fed rats. *Clin Exp Pharmacol Physiol* **43**, 372-378 (2016).
49. Guy, J. & Peters, M.G. Liver disease in women: the influence of gender on epidemiology, natural history, and patient outcomes. *Gastroenterol Hepatol (N Y)* **9**, 633-639 (2013).
50. Sekiya, M. et al. SREBP-1-independent regulation of lipogenic gene expression in adipocytes. *J Lipid Res* **48**, 1581-1591 (2007).
51. Liu, Y. et al. The Role of PPAR-δ in Metabolism, Inflammation, and Cancer: Many Characters of a Critical Transcription Factor. *Int J Mol Sci* **19** (2018).
52. Chatterjee, I. et al. Vitamin D receptor promotes healthy microbial metabolites and microbiome. *Sci Rep* **10**, 7340 (2020).
53. Penn, D.J., Zala, S.M. & Luzynski, K.C. Regulation of Sexually Dimorphic Expression of Major Urinary Proteins. *Front Physiol* **13**, 822073 (2022).
54. Lu, Y., Pang, Z. & Xia, J. Comprehensive investigation of pathway enrichment methods for functional interpretation of LC-MS global metabolomics data. *Brief Bioinform* **24** (2023).
55. Johnstone, T.C., Park, G.Y. & Lippard, S.J. Understanding and improving platinum anticancer drugs--phenanthriplatin. *Anticancer Res* **34**, 471-476 (2014).
56. Marcu, L.G. Gender and Sex-Related Differences in Normal Tissue Effects Induced by Platinum Compounds. *Pharmaceuticals (Basel)* **15** (2022).
57. Chen, W.Y. et al. Cisplatin Nephrotoxicity Might Have a Sex Difference. An analysis Based on Women's Sex Hormone Changes. *J Cancer* **8**, 3939-3944 (2017).
58. Nematbakhsh, M. et al. Gender difference in Cisplatin-induced nephrotoxicity in a rat model: greater intensity of damage in male than female. *Nephrourol Mon* **5**, 818-821 (2013).
59. Zhu, D., Montagne, A. & Zhao, Z. Alzheimer's pathogenic mechanisms and underlying sex difference. *Cell Mol Life Sci* **78**, 4907-4920 (2021).
60. Bresilla, D. et al. The sex-specific metabolic signature of C57BL/6NRj mice

during aging. *Sci Rep* **12**, 21050 (2022).
61. Raldiris, T.L., Perez, E., Donovan, E.K. & Dzierzewski, J.M. Cognitive control beliefs and cognitive functioning in mid- to late-life. *Br J Dev Psychol* **39**, 269-281 (2021).
62. Mauvais-Jarvis, F., Arnold, A.P. & Reue, K. A Guide for the Design of Pre-clinical Studies on Sex Differences in Metabolism. *Cell Metab* **25**, 1216-1230 (2017).
63. Bryant, C.D. The blessings and curses of C57BL/6 substrains in mouse genetic studies. *Ann N Y Acad Sci* **1245**, 31-33 (2011).
64. Wilson, K.A. et al. Evaluating the beneficial effects of dietary restrictions: A framework for precision nutrigeroscience. *Cell Metabolism* **33**, 2142-2173 (2021).
65. Simopoulos, A.P. & Van Itallie, T.B. Body weight, health, and longevity. *Ann Intern Med* **100**, 285-295 (1984).
66. van de Wouw, M., Schellekens, H., Dinan, T.G. & Cryan, J.F. Microbiota-Gut-Brain Axis: Modulator of Host Metabolism and Appetite. *J Nutr* **147**, 727-745 (2017).
67. Ghosh, T.S., Shanahan, F. & O'Toole, P.W. The gut microbiome as a modulator of healthy ageing. *Nat Rev Gastroenterol Hepatol* **19**, 565-584 (2022).
68. McGee, J.S. & Huttenhower, C. Of mice and men and women: Sexual dimorphism of the gut microbiome. *Int J Womens Dermatol* **7**, 533-538 (2021).
69. Eshraghi-Jazi, F. & Nematbakhsh, M. Sex Difference in Cisplatin-Induced Nephrotoxicity: Laboratory and Clinical Findings. *J Toxicol* **2022**, 3507721 (2022).
70. Rostami, B. et al. Effect of testosterone on Cisplatin-induced nephrotoxicity in surgically castrated rats. *Nephrourol Mon* **6**, e21546 (2014).
71. Horstman, A.M., Dillon, E.L., Urban, R.J. & Sheffield-Moore, M. The role of androgens and estrogens on healthy aging and longevity. *J Gerontol A Biol Sci Med Sci* **67**, 1140-1152 (2012).
72. Leifke, E. et al. Age-related changes of serum sex hormones, insulin-like growth factor-1 and sex-hormone binding globulin levels in men: cross-sectional data from a healthy male cohort. *Clin Endocrinol (Oxf)* **53**, 689-695 (2000).
73. Shin, M.S. et al. Long-term Surgical and Chemical Castration Deteriorates Memory Function Through Downregulation of PKA/CREB/BDNF and c-Raf/MEK/ERK Pathways in Hippocampus. *Int Neurourol J* **23**, 116-124 (2019).
74. Kim, J.Y., Yang, S.H., Kwon, J., Lee, H.W. & Kim, H. Mice subjected to uncontrollable electric shocks show depression-like behaviors irrespective of their state of helplessness. *Behav Brain Res* **322**, 138-144 (2017).
75. Kutlikova, H.H. et al. The effects of testosterone on the physiological response to social and somatic stressors. *Psychoneuroendocrinology* **117**, 104693 (2020).
76. Xia, J. & Wishart, D.S. MSEA: a web-based tool to identify biologically meaningful patterns in quantitative metabolomic data. *Nucleic Acids Res* **38**, W71-77 (2010).
77. Alseekh, S. et al. Mass spectrometry-based metabolomics: a guide for annotation, quantification and best reporting practices. *Nat Methods* **18**, 747-756 (2021).
78. Luo, Y.M. et al. Insights into the mechanisms of triptolide nephrotoxicity through network pharmacology-based analysis and RNA-seq. *Front Plant Sci* **14**, 1144583 (2023).
79. Rong, S. et al. The TIM-1:TIM-4 pathway enhances renal ischemia-reperfusion

839 injury. *J Am Soc Nephrol* **22**, 484-495 (2011).
840 80. Jiang, J. et al. Decoding the role of long noncoding RNAs in the healthy aging
841 of centenarians. *Brief Bioinform* **22** (2021).
842 81. Ederer, M.L. et al. Voluntary Wheel Running in Old C57BL/6 Mice Reduces
843 Age-Related Inflammation in the Colon but Not in the Brain. *Cells* **11** (2022).
844 82. Lueptow, L.M. Novel Object Recognition Test for the Investigation of Learning
845 and Memory in Mice. *J Vis Exp* (2017).
846 83. Cox, M.P., Peterson, D.A. & Biggs, P.J. SolexaQA: At-a-glance quality
847 assessment of Illumina second-generation sequencing data. *BMC*
848 *Bioinformatics* **11**, 485 (2010).
849 84. Kim, D., Langmead, B. & Salzberg, S.L. HISAT: a fast spliced aligner with low
850 memory requirements. *Nat Methods* **12**, 357-360 (2015).
851 85. Trapnell, C. et al. Differential gene and transcript expression analysis of RNA-
852 seq experiments with TopHat and Cufflinks. *Nat Protoc* **7**, 562-578 (2012).
853 86. Kumar, L. & M, E.F. Mfuzz: a software package for soft clustering of
854 microarray data. *Bioinformation* **2**, 5-7 (2007).
855 87. Lu, Y., Pang, Z. & Xia, J. Comprehensive investigation of pathway enrichment
856 methods for functional interpretation of LC–MS global metabolomics data.
857 *Briefings in Bioinformatics* **24** (2022).
858 88. Su, G.-H. et al. Radiogenomic-based multiomic analysis reveals imaging
859 intratumor heterogeneity phenotypes and therapeutic targets. *Science Advances*
860 **9**, eadf0837 (2023).
861

862 **Author Contributions**

863 J.J. conceived and designed this study; J.J. and W.W. wrote and revised this manuscript;
864 S.Y. and F.L. provided necessary resources to this study; J.J. performed the
865 metabolomics, RNA-seq analysis, and the western blot assay; N.G. and X.G performed
866 the metabolomics analysis; Y.W. and G.W. performed the animal behavior tests; J. Q.,
867 and K. G. performed the sham/castration procedure; J.J., Y.W., G.W., J. Q., K. G., X.G
868 and Y.L. did the mouse colony and tissue samples collection.

869

870 **Acknowledgement**

871 We acknowledge Ms. Jiahui Liu for her generous help for sample collection and Dr.
872 Xinhui Liu for his kind help for assessing renal injury scores. This work was supported
873 by Shenzhen Science and Technology Program (Grant No.RCBS20210706092341003)
874 to J.J.

875

876 **Declaration of interests**

877 The authors declare that none of them have competing interests.

878

879 **FIGURES**

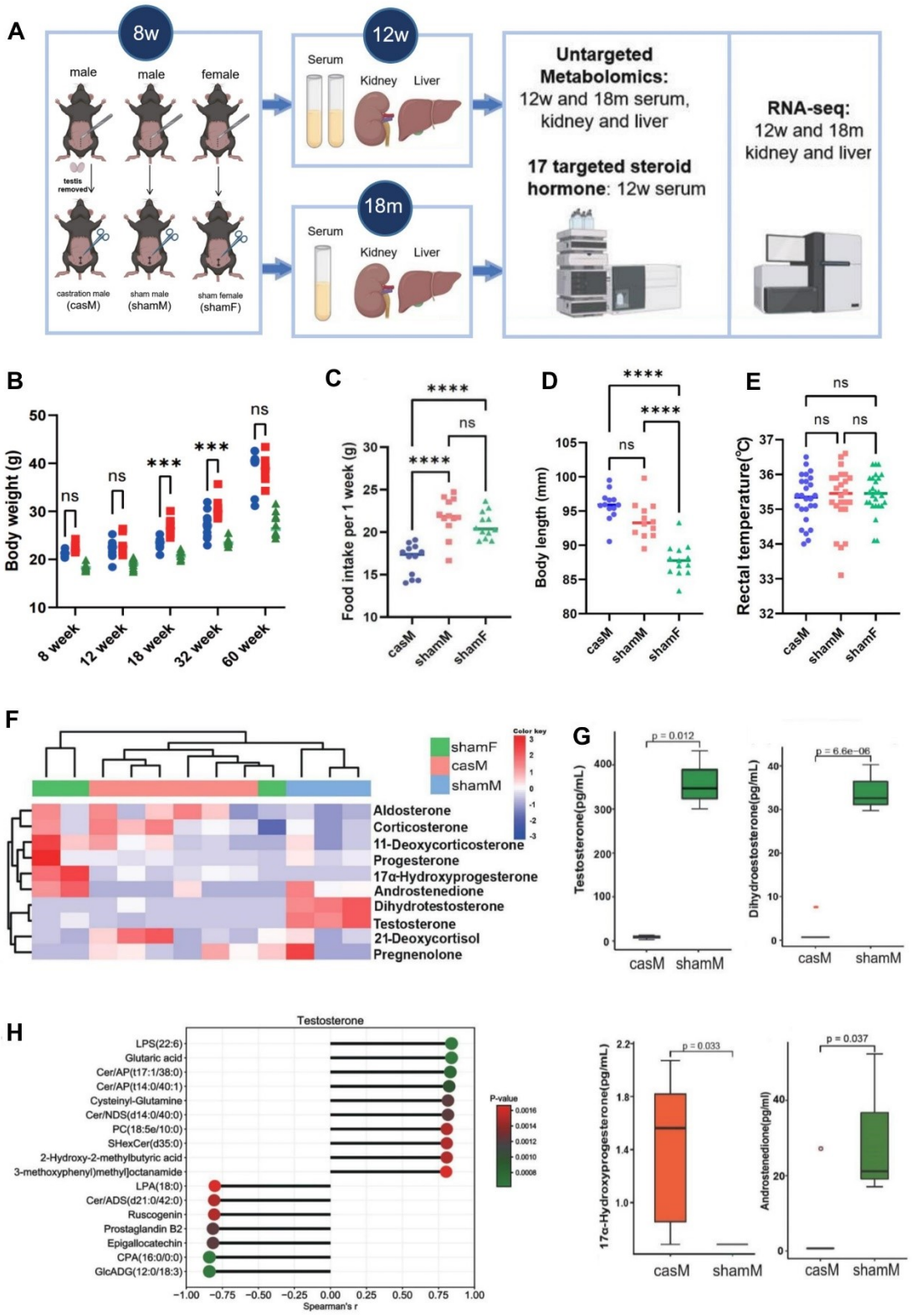

880

881 **Figure 1. Overall study design as well as phenotypic tests and steroid hormone**
882 **spectrum of castration mice.** (**A**) Graphic illustration of the overall experimental
883 design. (**B**) Body weight of casM, shamM and shamF mice from 8 to 60 weeks (n = 13,
884 12, 13 for casM, shamM, and shamF, respectively; unpaired students' t-test,***p <

0.001, ns: not significant) (**C**) Significant less food intake was observed in casM group by One-Way ANOVA, ****$p < 0.0001$ (**D-E**) non-significant difference among the 3 groups of mice was observed in (**D**) body length at 27 weeks old; (**E**) rectal temperature at 30 and 32 weeks old; (**F**) Hierarchical cluster heatmap of z-score standardized expression levels of 10 detectable steroid hormones among shamM, casM and shamF; (**G**) Comparisons of the quantitative levels of testosterone, dihydroestosterone, 17-hydroxyprogesterone and androstenedione between shamM and casM (unpaired students' t-test, *p*-values were shown on top); (**H**) List of compounds highly correlated with TS (Spearman's $|r| \geq 0.8$, $p \leq 0.001$). Median line was shown for G.

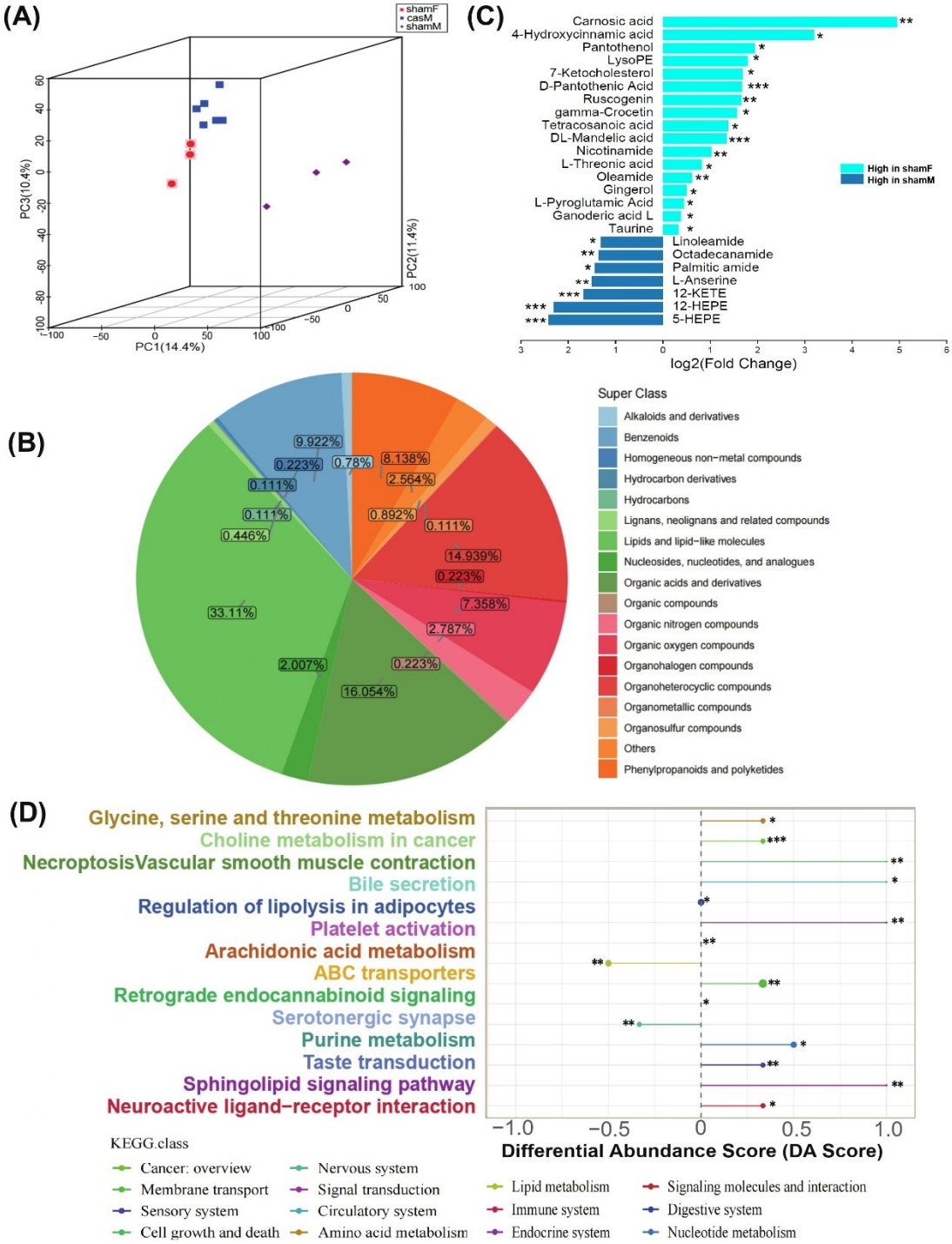

Figure 2. Characterizations of the 12w serum metabolomics. (**A**) PCA clustering of the serum untargeted metabolomics among casM, shamM and shamF; (**B**) Categories of the 1495 12w serum metabolites with high quality MS^2 annotations; (**C**) Representative SAMs between shamM and shamF that related with aging and healthy aging (unpaired students' t-test, $*p < 0.05$, $**p < 0.01$, $***p < 0.001$); (**D**) Differential abundance (DA) scores were calculated for the significant enrichment terms between shamM and shamF ($*p < 0.05$, $**p < 0.01$, $***p < 0.001$).

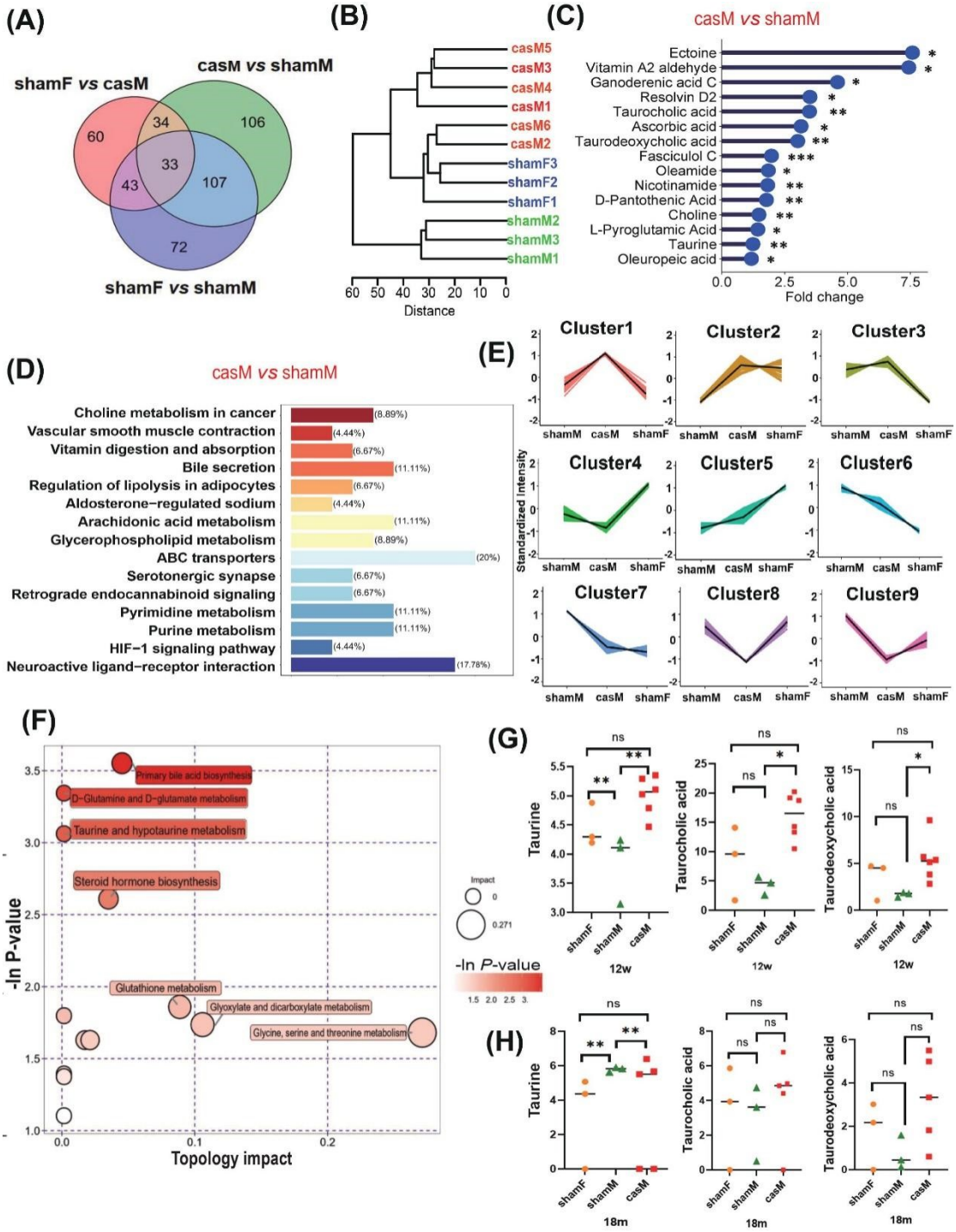

Figure 3. Identification of castration-specific metabolomic features in 12w mice. (**A**) Venny diagram of the serum SAMs identified from "shamF *vs* ShamM", "shamF *vs* casM" and "casM *vs* ShamM"; (**B**) Hierarchical clustering tree of different mouse groups using levels of compounds as input; (**C**) Representative food derived SAMs between casM and shamM (unpaired students' t-test, $*p < 0.05$, $**p < 0.01$, $***p < 0.001$); (D) Barplot of the KEGG enrichment terms using SAMs of "casM *vs* ShamM", percentage of hit compounds to total SAMs was calculated for each term; (**E**)

Expression patterns of merged SAMs among casM, shamM and shamF analyzed using mfuzzing clustering. Clusters 1 and 8 distinctively represent metabolites that are, respectively, highly and lowly detected specifically in casM. (**F**) Significantly enriched KEGG terms of metabolites highly expressed metabolites in casM (cluster 1 in **E**) calculated by topology-based pathway enrichment with topology impact shown in x-axis; (**G-H**) Comparisons of taurine, taurocholic acid and taurodeoxycholic acid among 12w (**G**) and 18m (**H**) shamF, shamM and casM (One-Way ANOVA, $*p < 0.05$, $**p < 0.01$, ns: not significant). For G and H, Tukey correction was used for correction of multiple comparisons and median lines were shown.

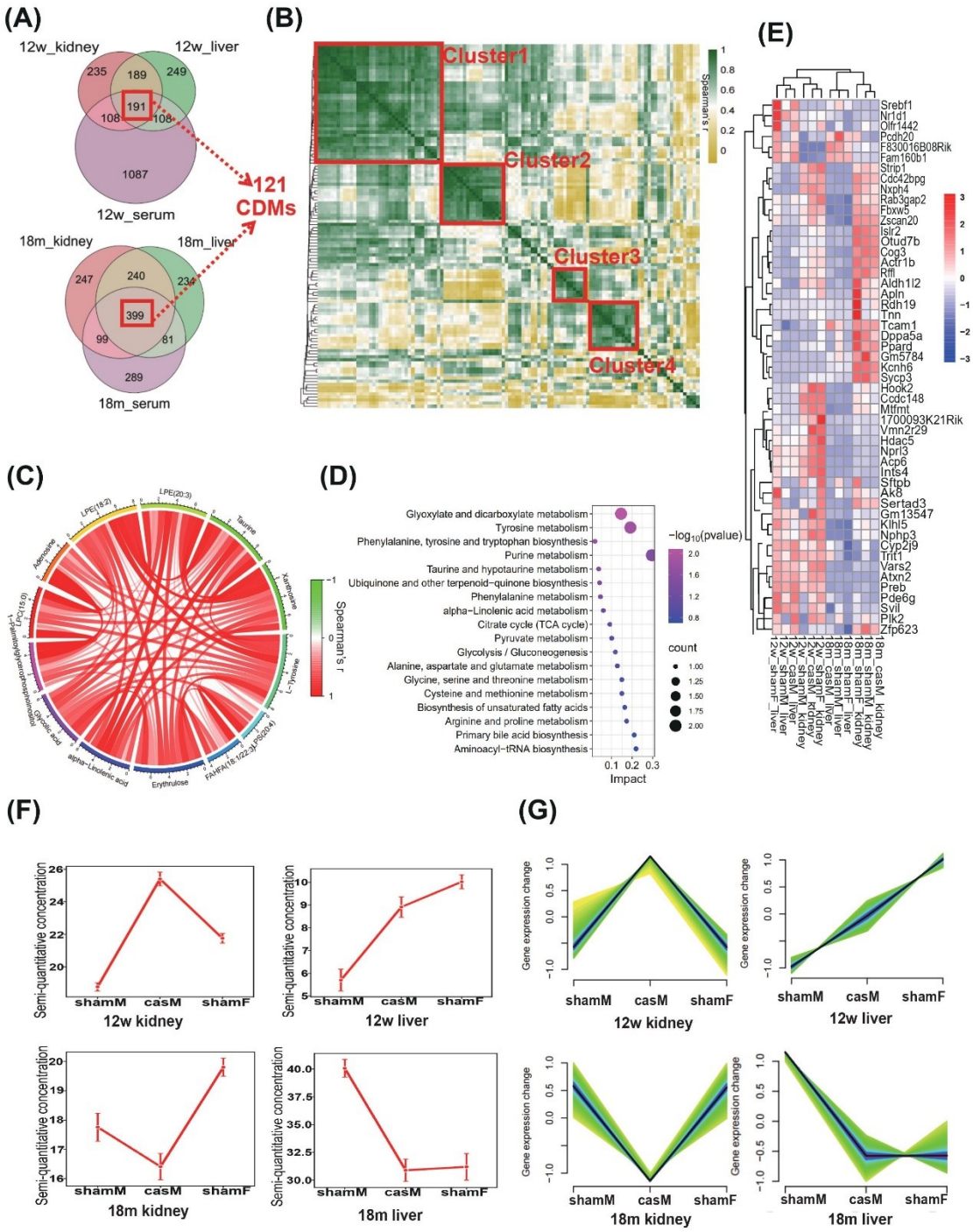

Figure 4. Co-expression analysis across serum, livers and kidneys identifies potential taurine-related regulators. (**A**) Venn diagram of detected compounds among serum, livers and kidneys across all the mouse groups at 12w and 18m, 121 commonly detected compounds (CDBs) were identified; (**B**) Co-expression analysis of the 121 CDBs revealed four major consensus clusters; (**C**) Correlation circos plot of the cluster 4 compounds in **B**; (**D**) Topology-based pathway enrichment analysis of the cluster 4 compounds in **B**, x-axis is the topology enrichment impact of hinted

930 compounds; (**E**) Hierarchical cluster heatmap of z-score standardized expression levels
931 of 51 taurine related genes in 12w and 18m kidneys and livers among shamM, shamF
932 and casM mice. Genes selectively reduced in 18m tissues are highlighted in red; (**F**)
933 Trends of taurine levels with standard deviation (SD) among shamM, shamF and casM
934 across liver and kidney tissues in 12w and 18m mice; (**G**) Mfuzzing clustering of the
935 51 taurine co-expressed genes across liver and kidney tissues in 12w and 18m mice.
936

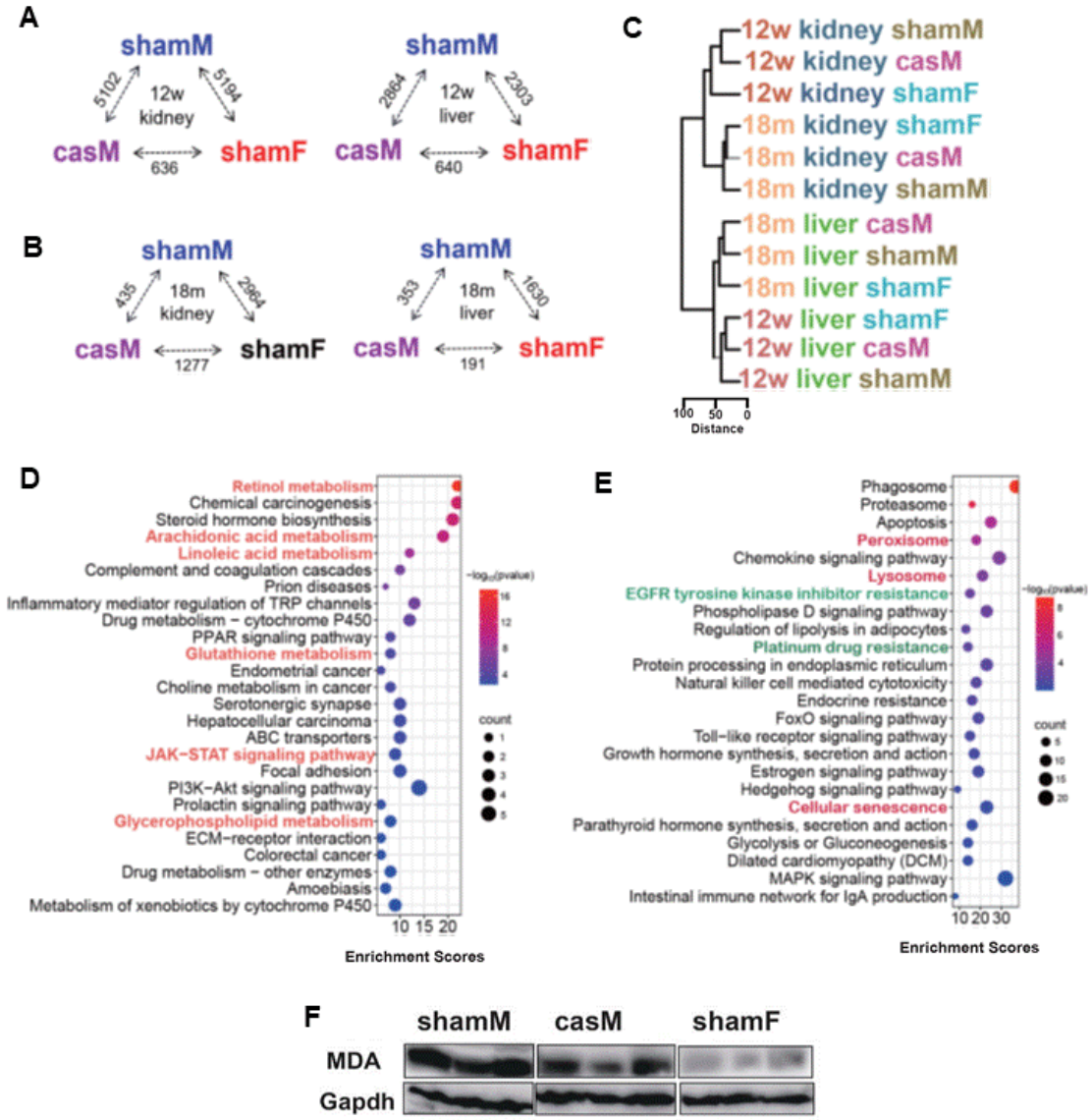

Figure 5. Joint metabolomic-transcriptomic analysis reveals a stronger capacity of defensing lipid peroxidation in female and castrated male. (**A-B**) The numbers of DEGs among livers and kidneys tissues of shamM, shamF and casM mice collected at 12w (**A**) and 18m (**B**); (**C**) Hierarchical clustering of 12w and 18m liver and kidney samples demonstrating casM's closer alignment with shamF than sham; (**D, E**) Representative significantly enriched KEGG pathways in 18m liver samples from 'casM *vs* ShamM,' (**D**) and 'shamF *vs* ShamM' (**E**), identified by joint transcriptomic-metabolomic analysis using DEGs and SAMs. Pathways marked in orange indicate common terms between these two comparisons. (**F**) Immunoblotting of MDA in 18m livers;

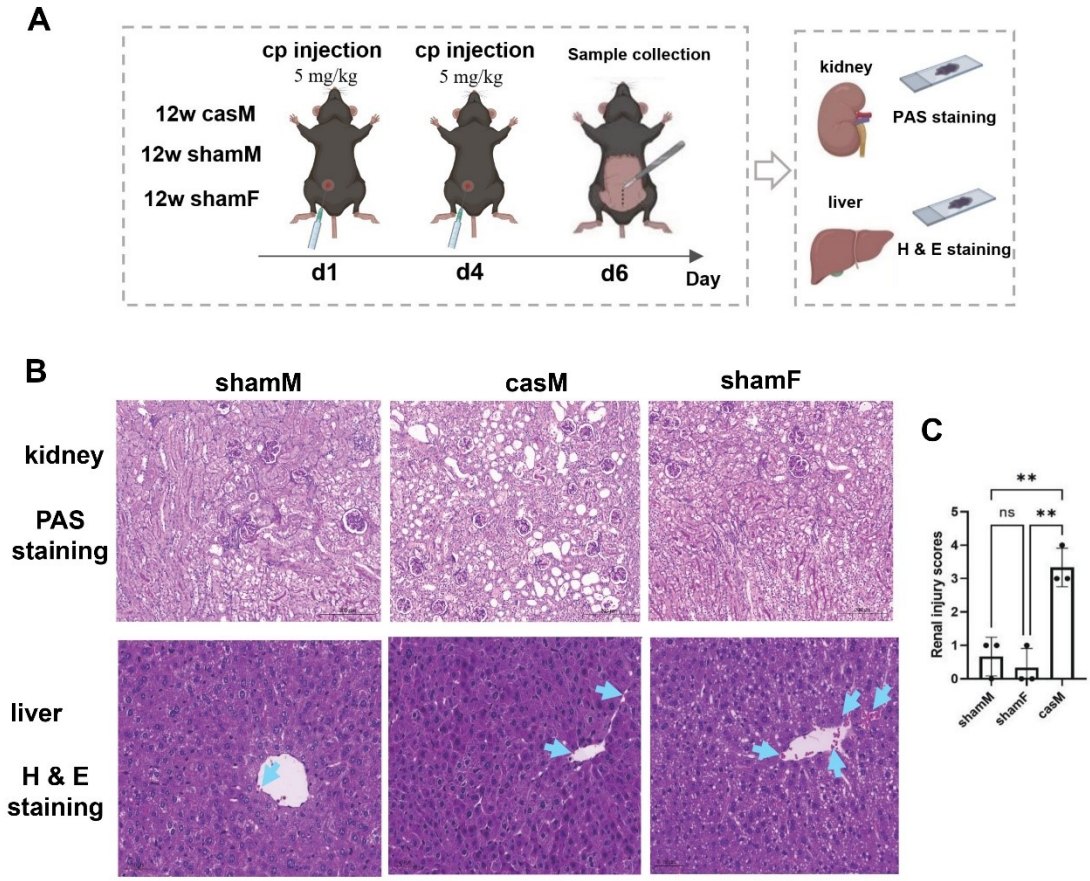

Figure 6. Illuminating sex hormone influence in cisplatin toxicity through castration models. (A) Graphic illustration of the experimental design; (**B**) PAS staining of kidneys (upper panel) and H & E staining of livers (lower panel) in 12w mice (4 week post castration/sham procedure) with cisplatin treatment, blue arrows indicate representative injury spots in livers; (**C**) Bar plots of renal injury scores in three groups of mice by One-Way ANOVA test (Tukey correction was used for correction of multiple comparisons, $^{**}p < 0.01$, ns: not significant).

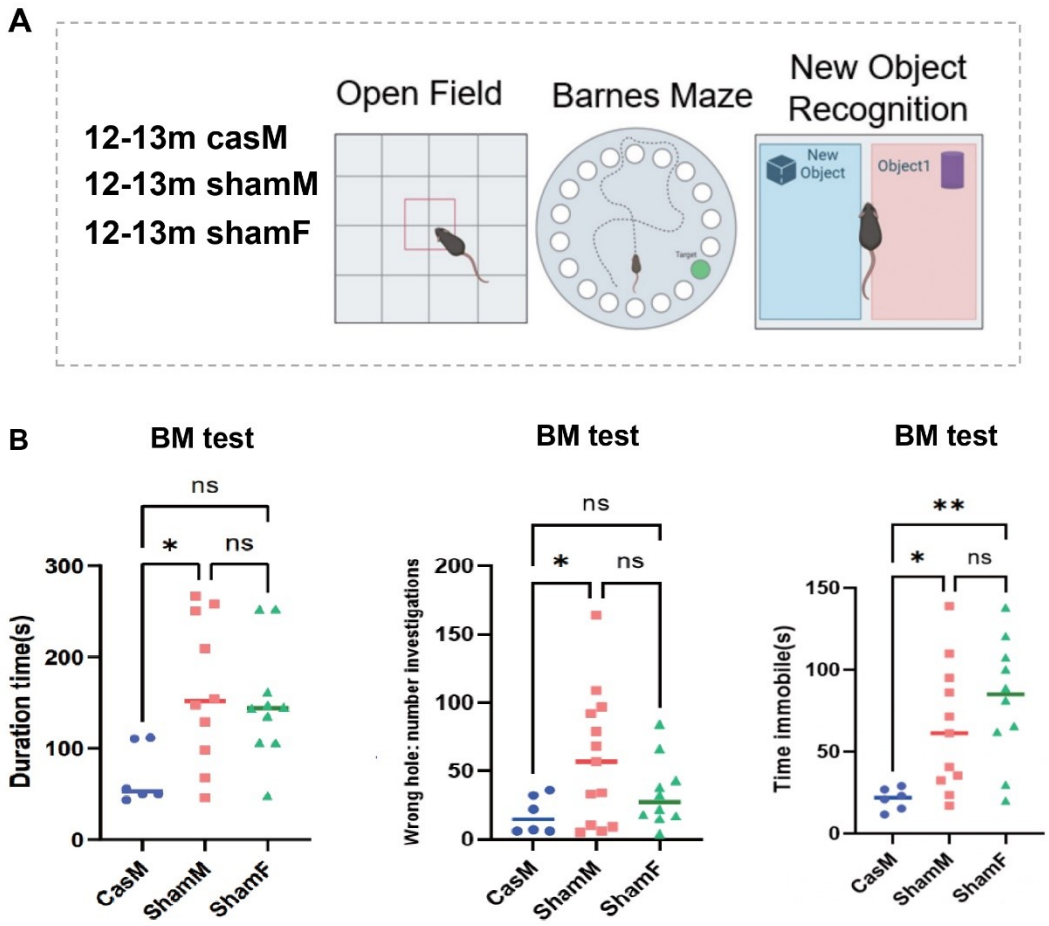

Figure 7. Aging-related cognitive function tests among three groups of mice. (A) Graphic illustration of the behavioral tests; (**B**) Analysis of BM tests results: duration time that mice have spent to find the correct target escape hole (left panel), exploration of wrong holes numbers (middle panel), and immobile time during the test (right panel) among casM (n=6), shamM (n= 13) and shamF (n = 10) by One-Way ANOVA, $*p < 0.05$, $**p < 0.01$, ns: not significant. For Figure 1C & E-G, Tukey correction was used for correction of multiple comparisons and median lines were shown.